

Defect analysis on the evolution of vertical graphene nanosheets grown by electron cyclotron resonance - plasma enhanced chemical vapor deposition

Subrata Ghosh^{1,*}, K. Ganesan^{1,†}, Shyamal R. Polaki¹, T.R. Ravindran¹, Nanda Gopala Krishna², M. Kamruddin¹ and A.K. Tyagi¹

¹ Materials Science Group, Indira Gandhi Centre for Atomic Research, Kalpakkam - 603102, India.

² Corrosion Science and Technology Group, Indira Gandhi Centre for Atomic Research, Kalpakkam - 603102, India.

Abstract

We report catalyst-free direct synthesis of vertical graphene nanosheets (VGNs) on SiO₂/Si and quartz substrates using microwave electron cyclotron resonance - plasma enhanced chemical vapor deposition. The evolution of VGNs is studied systematically at different growth stages. Raman analysis with respect to growth time reveals that two different disorder-induced competing mechanisms contributing to the defect band intensity. The VGNs grown on SiO₂/Si substrates predominantly have both the vacancy-like and hopping defects. On the other hand, the VGNs grown on quartz substrates contain mainly boundary-like defects. XPS studies also corroborate Raman analysis in terms of defect density and vacancy-like defects for the VGNs grown on SiO₂/Si substrates. Moreover, the grown VGNs exhibit a high optical transmittance from 95 to 78 % at 550 nm and the sheet resistance varies from 30 to 2.17 kΩ/□ depending on growth time.

1. Introduction

Over the past few decades, carbon nanostructures opened a new window to scientific community due to their unique structures and exotic physical properties [1-3]. The graphene, newborn in carbon wonderland, has fuelled academic and industrial interest due to its unusual

* Electronic mail : subrataghosh.phys@gmail.com (Subrata Ghosh)

† Corresponding author. Tele.: +91-44-27480500 Extn: 22514. Email : kganesan@igcar.gov.in (K. Ganesan)

electronic and mechanical properties, in particular, ballistic and tunable transport properties [3-5]. To realize its potential for future nanoelectronics, a reliable, fast and reproducible synthesis technique is necessary. The mass production of large area graphene is the most challenging goal for device applications. The general approaches to graphene synthesis are exfoliation (mechanical or chemical), epitaxial growth, graphene oxide (GO) reduction and chemical vapor deposition (CVD) [6]. Among them, thermal CVD is the most popular to overcome the limitation of scalability. The interaction between carbon π orbital and surface atoms of the metal substrates (Cu, Ni) plays the major role in graphene growth [5, 7]. However, the CVD grown graphene has to undergo a major hurdle of transferring onto a dielectric substrate before entering into devices. The transfer process introduces impurities and it could degrade the quality of the graphene. For example, the organic solvent polymethyl methacrylate (PMMA) used for transfer can be a source of *p*-type doping element, and also dissolving the PMMA residue completely from graphene is not easy [8].

Catalysis-free direct synthesis of graphene on dielectric substrates, compatible with complementary metal oxide semiconductor technology, is a challenging task. Recently, the direct growth of graphene on dielectric substrates are explored by thermal CVD, yet with limited success [9,10]. Alternatively, the plasma enhanced CVD (PECVD) have already shown its potential in growing various carbon nanostructures. The main advantages of PECVD are that it is catalyst free, short growth time can be carried out at relatively low temperatures and is amenable to doping. In addition, the technique is ideal for uniform large area and conformal coatings. There are several reports on growth of carbon nanostructures by various plasma based techniques such as microwave PECVD, dc plasma discharge, ICP-plasma, thermal plasma jet systems [11-20]. However, the PECVD grown samples are found to be vertically oriented which are attributed to the in-built electric fields associated with plasma [15]. Due to the structural characteristics with high aspect ratio and large 3D networks, the vertical graphene nanosheets (VGNs), also called as carbon/graphene nanowalls/nanosheets/naoflakes, are excellent candidates for applications in field emission, fuel cells, chemical and biosensors, energy storage devices [12,14,16,17]. In order to use them in an efficient way, a detailed understanding of growth mechanism and their structural evolution are necessary.

Earlier studies on growth of carbon nanotubes by plasma based techniques using metallic catalyst lead to the invention of VGNs [15]. Several groups have explored the growth of graphene/carbon nanosheets on catalytic as well as non-catalytic metal surfaces. However, synthesis of VGNs on semiconducting and dielectric substrates is rare. In an excellent review, Bo *et al* [11] summarized the influence of various key process parameters such as type of feedstock gas and composition, microwave power, electric field, temperature and pressure on the synthesis of VGNs and also the growth model for the vertical orientation of nanosheets on various types of substrates. However, it should be noted that still, there is no unified theory to unveil the growth mechanism and to optimize the process parameters for a given plasma source [11]. Further, the PECVD synthesized materials suffer from large amount of defects due to ion bombardment from the high density plasma. Hence, it is very important to gain knowledge over the defect formation mechanism with respect to the process parameters in order to minimize defects. Raman spectroscopy is an excellent tool to investigate the defects in carbon materials. Though almost all previous reports on plasma based graphene synthesis include Raman data, a detailed analysis of defects and disorder, such as nature of defects, quantification of defect concentration and their correlation with growth mechanism, are scarce.

In view of proven capability to synthesis electronic grade carbon materials, we consider microwave electron cyclotron resonance plasma enhanced chemical vapor deposition (ECR-CVD) as a promising technique to fabricate VGNs on SiO₂/Si and quartz substrates [17]. In the present study, we discuss the catalyst-free synthesis of VGNs and their structural analysis using scanning electron microscopy (SEM), Raman spectroscopy and x-ray photoemission spectroscopy (XPS) techniques. A quantitative defect analysis is carried at various stages of growth and the types of defects associated with the two different substrates are identified. XPS studies are also carried out to reveal surface chemistry and support defect analysis. Further, electrical and optical properties of VGNs are studied at room temperature. Overall, a comprehensive understanding on the growth mechanism of VGNs on SiO₂/Si and quartz substrates and its defects analysis are presented.

2. Experimental methods

2.1 Growth of VGNs by ECR-CVD

The VGNs are deposited on SiO₂/Si and quartz substrates under CH₄/Ar plasma in an ECR-CVD reactor. The schematic of the ECR-CVD system is given in Fig. 1. The system consists of a microwave source operating at 2.45 GHz with maximum power of 1.2 KW and an electromagnet generating a magnetic field of 875 Gauss which satisfies the ECR condition. The source gas CH₄ is sent through a circular showerhead that uniformly injects gas into the reaction chamber. An adjustable substrate holder with heater allows manipulation of the distance between the quartz window and the substrate. Growth time ranges from 10 sec to 45 min.

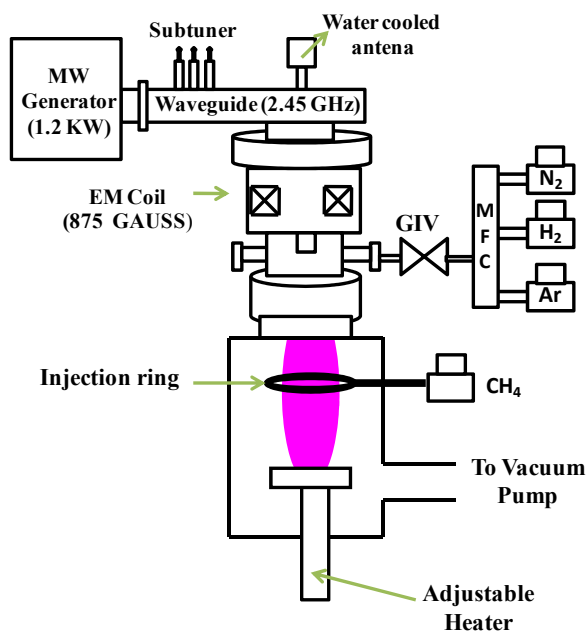


Fig.1- Schematic of the ECR-CVD reactor chamber

Ultrasonically cleaned substrates are loaded into the substrate holder and the chamber is evacuated down to a base pressure 5×10^{-6} mbar by a turbomolecular pump. The substrate temperature is increased to 750 °C and after 20 minutes, the substrates are pre-cleaned by Ar plasma under 20 sccm Ar flow for 10 min at 200W microwave power. After pre-cleaning the substrates, CH₄ is fed into the chamber through circular showerhead at 2.5 sccm flow rate, subsequently Ar flow is reduced to 2.5 sccm. The growth experiments are then performed at the

microwave power of 400 W. The operating pressure of the reactor chamber is maintained about 1×10^{-3} mbar. Following the growth, the plasma is turned off and the substrates are annealed for 10 min at the same growth temperature. Finally, the samples are cooled down to room temperature and taken out for characterization.

2.2 Characterization

The VGNs morphology is studied using a field emission scanning electron microscope (SEM, Supra 55, Zeiss). The structural properties, in terms of defects and disorder, are evaluated by micro-Raman spectroscopy (Renishaw inVia, UK) with 514 nm laser and accumulation time of 10 seconds with 100X objective lens. Surface chemical analysis of the VGNs are carried out by x-ray photoelectron spectroscopy (XPS, M/s SPECS, Germany). Sheet resistance is measured in van der Paw geometry using Agilent B2902A precision source/measure unit. The optical transmittance is measured by ultraviolet-visible spectroscopy (UV-Vis, Avantes AvaLight-DH-S-BAL) in the range 200-800 nm for the VGNs grown on quartz substrates.

3. Results and discussion

3.1 SEM analysis

The surface morphologies of the VGNs grown on SiO_2/Si substrates are characterized by SEM at different stages of growth (Fig. 2 (a-d)). Fig. 2e shows the cross sectional SEM image of VGNs grown for 45 minutes and it has the height of 48 nm. The variation in number density and height with duration of growth is given in Fig 2f. At the very early stage of growth, of about 10 seconds duration, the film consists of many island structures over the smooth substrate as seen in Fig. 2a. It should be noted that even at this very short duration of growth, the film is electrically conductive with sheet resistance of about $30 \text{ k}\Omega/\square$. This indicates the initial formation of uniform planar graphitic structure followed by a change to island structure as an outcome of stress relaxation process [19]. As the growth time increases, the graphene structures continue to grow further vertically over the stress relaxed regions. With increase in growth time, a decrease in number density of the vertically aligned sheets and increase in their height are observed, as seen in Fig 2 (a-f).

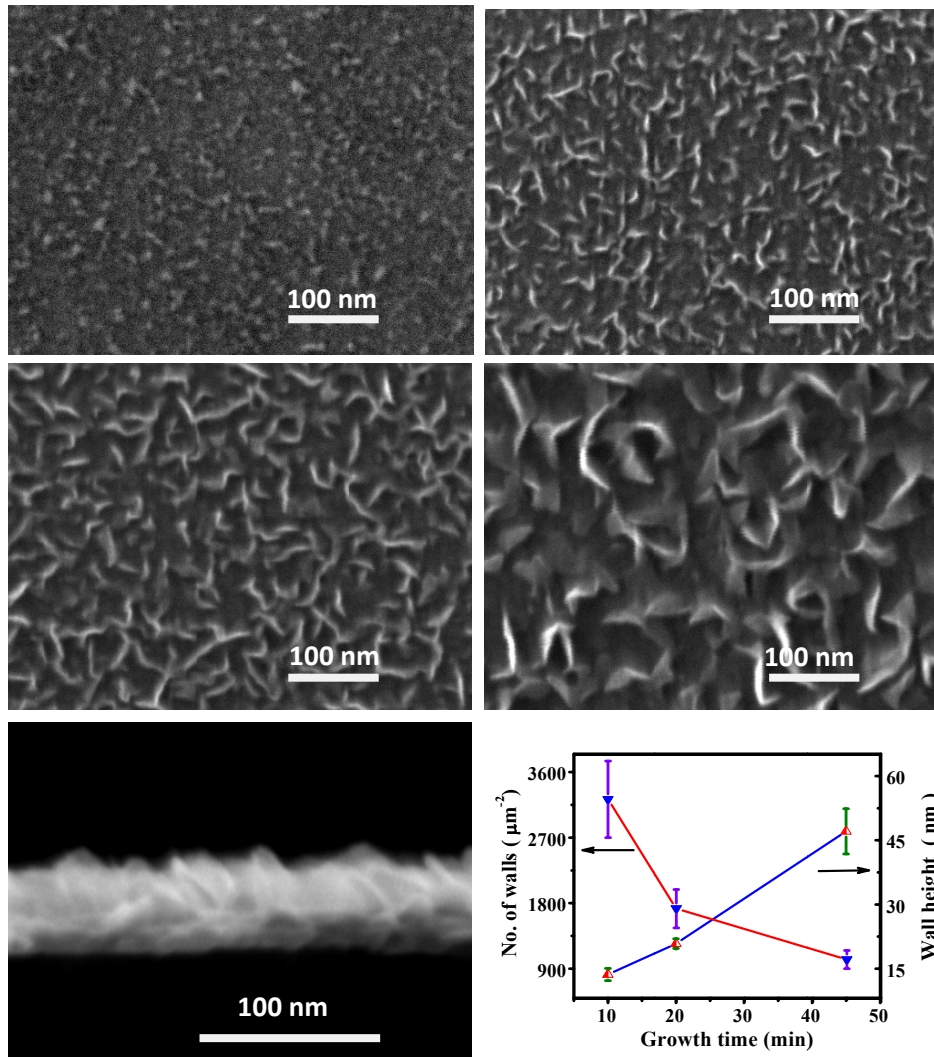


Fig. 2- The SEM micrographs of the VGNs grown at different duration of (a) 10 sec (b) 10 mins (c) 20 mins and (d) 45 mins. (e) cross-sectional SEM micrograph of the film grown for 45 mins (f) The plot indicates the wall density and wall height as a function of growth duration.

The direct growth of VGNs on dielectric substrates can be understood by the following steps. During pre-cleaning procedure, the Ar^+ ions in the plasma removes surface contaminations and partial lattice oxygen in SiO_2/Si surface, which creates dangling bonds on dielectric substrates for carbon nucleation. During growth, the microwave energy in ECR-CVD creates a high density plasma with variety of free radicals in several combinations such as CH_x , C_xH_y , C_2 dimers, Ar-H and atomic hydrogen [11]. Based on the results of SEM analysis, we understand

that at the early stage of growth (< 10 sec.), the carbon and hydro-carbon radicals get adsorbed at the active sites and form 3D nanocrystalline graphite (nanographite) islands due to surface diffusion of carbon species. At about 10 sec, nanographite islands coalesce to form electrically continuous nanographite layers parallel to the substrate surface. During the coalescence of nanographitic islands, the stress release occurs at the interface between the nanographite grain boundaries. Thus, the stress relaxation process results in the protrusion of carbon atoms around the grain boundaries which initiates the vertical growth of graphene nanostructures. Further increase in growth time, brings more carbon ad-atoms to the growing film and carbon diffusion takes place in the planar regions as well as the vertically growing graphene nanosheets. However, the carbon atoms diffusing to the edge of vertical graphene binds well due to strong in-plane C-C covalent bond and grow normal to the substrate. On the other hand, the carbon species arriving at planer region are re-evaporated due to the weak van der Waals force between the graphene layers. Meanwhile, the atomic hydrogen generated from CH_4 by microwave energy also etches out amorphous carbon (a-C), sp^3 -C and sp^2 -C at different rates. This simultaneous growth and etching process make the VGNs to increase the height and decrease the number density with growth time. Further, a detailed Raman analysis and XPS studies are carried out to support the growth mechanism discussed here.

3.2 Raman analysis

Raman spectroscopy is a well-established and powerful technique for structural characterization of carbon-based materials. In addition to ascertaining the crystalline state, it is useful to investigate defects and disorder in the family of carbon materials [13, 21,23-30]. Here, we analyze the amount and type of defects formed during the evolution of VGNs on SiO_2/Si and quartz substrates. Fig. 3 shows a typical Raman spectrum of VGNs grown by ECR-CVD. The spectrum consists of two prominent bands - G and 2D (also called as G') at ~ 1580 and 2700 cm^{-1} respectively, which is signature of graphitic structure. Also, it consists of one phonon defect-assisted processes such as D, D' and D'' bands and two phonon defect-assisted processes such as $2\text{D}'$, $\text{D}+\text{D}'$ and $\text{D}+\text{D}''$ bands. The D, D' , $2\text{D}'$, D'' , $\text{D}+\text{D}'$ and $\text{D}+\text{D}''$ bands are activated only by defects and these bands are absent in pristine graphene. Also, these bands are strongly

dispersive with excitation energy due to the presence of defects and disorder [21]. The D band ($\sim 1350 \text{ cm}^{-1}$) and D' band ($\sim 1620 \text{ cm}^{-1}$) originate from an inter-valley and intra-valley double resonance (DR) process respectively. The 2D' band is the overtone of D' band and appears at $\sim 3250 \text{ cm}^{-1}$. The peak at $\sim 2485 \text{ cm}^{-1}$ is assigned to D+D'' band which is due to the combination of D phonon and the zone boundary phonon corresponding to LA branch at 1100 cm^{-1} [21]. The weak and broad band around 1100 cm^{-1} , as shown in inset of Fig. 3a, can also be associated with a bond stretching mode of sp^3 sites [22].

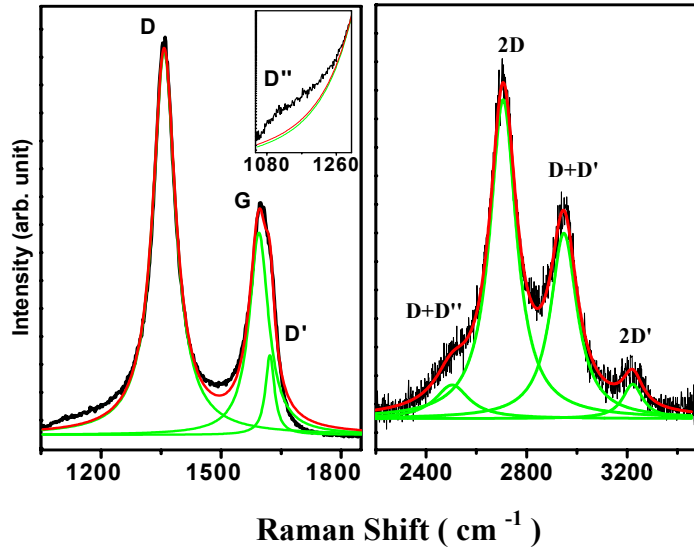


Fig.3- Typical Raman spectrum of VGNs grown on SiO_2/Si and its deconvolution with Lorentzian line shape.

Fig. 4a shows the Raman spectra of VGNs grown on SiO_2/Si substrates for different durations ranging from 10 sec to 45 minutes. Similar spectra are observed for films grown on quartz substrates and not shown here. The Raman spectrum of the film grown for 10 seconds shows a very broad D and G bands and nearly negligible intensity of 2D band indicating a more disordered structure. The intensity of the D, G and 2D bands increases with growth time. Also, the FWHM of D, G and 2D bands decreases with growth time (shown in Fig. 4b). A significant intensity in 2D band is observed when the growth time exceeds 10 minutes as shown in Fig. 4a. Further, the increase in growth time shifts the G band position $[\text{Pos}(\text{G})]$ from 1598.0 (1598.7) to 1590.7 (1588.8) cm^{-1} for the VGNs grown on SiO_2 (quartz) substrates indicating the improvement in crystallinity with growth time (Fig. 4c) [23]. The other two bands, D and 2D, do

not show any systematic change in peak position with respect to growth time. Also, the intensity ratio of 2D to G band (I_{2D}/I_G) increases with respect to growth as shown in Fig 4c. The observed FWHM of G and 2D bands of the films grown for 45 mins on SiO₂/Si (quartz) substrates are about 58 (38) and 95 (80) cm⁻¹ respectively. The observed large D band intensity is due to the presence of disorder which arises from large amount of edge states, sp³ bonded C-H species, nanographitic base layer and ion induced defects from the plasma during growth.

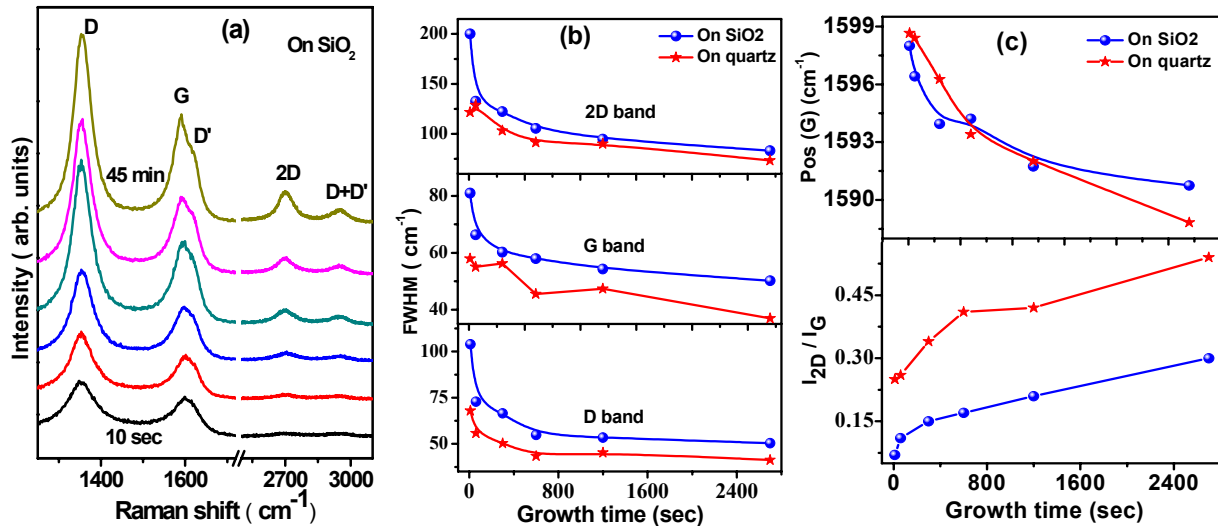


Fig.4- (a) Evolution Raman spectra of VGNs at different growth duration of 10 sec, 1, 5, 10, 20 and 45 mins. The spectra are stacked up vertically with increasing growth time (b) FWHM of D, G and 2D- bands and (c) The variation of G-band position and I_{2D}/I_G with respect to growth time. The solid lines in Fig4b, 4c are guide to eye.

Defects play a crucial role in determining the physical and mechanical properties of the mesoscopic structures. In order to engineer the desired properties of graphene, it is important to study the correlation between the type of defects and its Raman scattering process. In recent times, considerable efforts are taken to investigate the nature of defects and its quantification on graphene by introducing specific type of defects through Ar⁺-ion bombardment or plasma surface modification [13, 24-28]. In a disordered graphitic system, it is known that the intensity ratios of D to G (I_D/I_G) provide a measure of defects / disorder in the films. When defect density is relatively large as in the case of present study, it is better to take the peak intensity ratio rather

than peak area ratio. The latter is more accurate for a system with low defect concentration [27, 28]. According to the resonant Raman scattering theory, the intensity of defect bands (I_D , $I_{D'}$) not only depends on the amount of defects but also the type of defects associated with it. The ratio of $I_D/I_{D'}$ would provide information about the type of defects present in the material. If the ratio of $I_D/I_{D'}$ is 13, it indicates the presence of sp^3 related defects, and similarly, 10.5 corresponds to hopping defects, 7 for vacancy-like defects, 3.5 for boundary-like defects and 1.3 represents the on-site defects in graphene [28,29]. In fig. 5, the plot of I_D/I_G versus $I_{D'}/I_G$ shows a linear behavior, agree well with the earlier reports [29]. The observed slopes ($I_D/I_{D'}$ ratio) are found to be 8.57 ± 2.86 and 3.98 ± 0.68 for the VGNs grown on SiO_2/Si and quartz substrates respectively. The slopes indicate the existence of combined vacancy-like and hopping defects for the VGNs grown on SiO_2/Si substrates and boundary-like defects for the VGNs grown on quartz substrates. The different values of $I_D/I_{D'}$, I_{2D}/I_G and FWHM of phonon modes (D, G, 2D) for the VGNs grown on SiO_2/Si and quartz are due to dissimilar adsorption abilities of incoming carbon ions on different substrates [16].

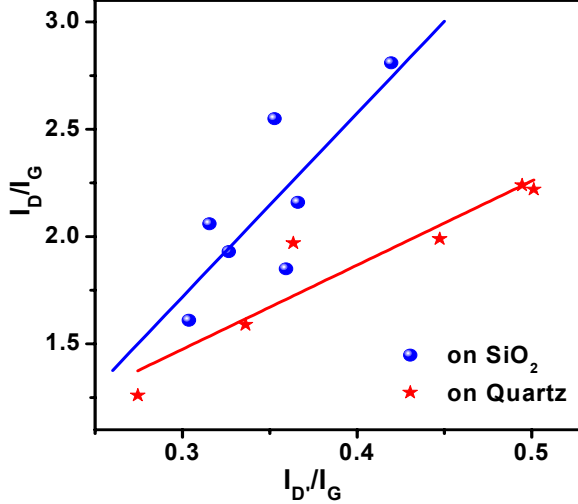


Fig.5- The plot of I_D/I_G vs $I_{D'}/I_G$ for the VGNs grown on SiO_2/Si and quartz substrates. The slope, 8.57 ± 2.86 , indicates combined vacancy-type and hoping defects for films grown on SiO_2/Si , and 3.98 ± 0.68 represents boundary-like defects for the film on quartz substrates.

Fig. 6a shows the variation of I_D/I_G with respect to growth time. It indicates that the I_D/I_G ratio has a non-monotonic dependence on growth time, increasing with growth time upto 10

minutes, and then decreases beyond 10 minutes. However, as discussed earlier (Fig 4b), the decreased FWHM of D, G, 2D bands signify the reduction of defects and disorder in the VGNs with growth time. Hence, the non-monotonic behavior of I_D/I_G ratio with growth time suggests the existence of two disorder-induced competing mechanisms contributing to the D band intensity. This behavior can be understood in terms of the well established defects and disorder model, amorphization trajectory of graphitic materials, proposed by Ferrari and Robertson [30]. The transformation of highly sp^2 bonded graphite into highly sp^3 bonded tetrahedral amorphous carbon (ta-C) through three stages viz. (1) graphite to nanocrystalline graphite [low defect (LD)]; (2) nanocrystalline graphite to low sp^3 a-C [high defect (HD)] and (3) low sp^3 a-C to high sp^3 ta-C. The mechanism for the formation of D band intensity is different in each stage. It is established that the I_D is directly proportional to amount of defects in stage 1 and inversely proportional to defects in stage 2, and also I_G is always proportional to the amount of sp^2 rings present in the sample [25, 29]. Hence, we attribute the non-monotonic behavior of I_D/I_G with growth time to the transformation of defects and disorder from stage 2 to stage 1. Thus, the VGNs grown for ≤ 10 min and $>$ than 10 minutes follow the stage 2 and stage 1 respectively.

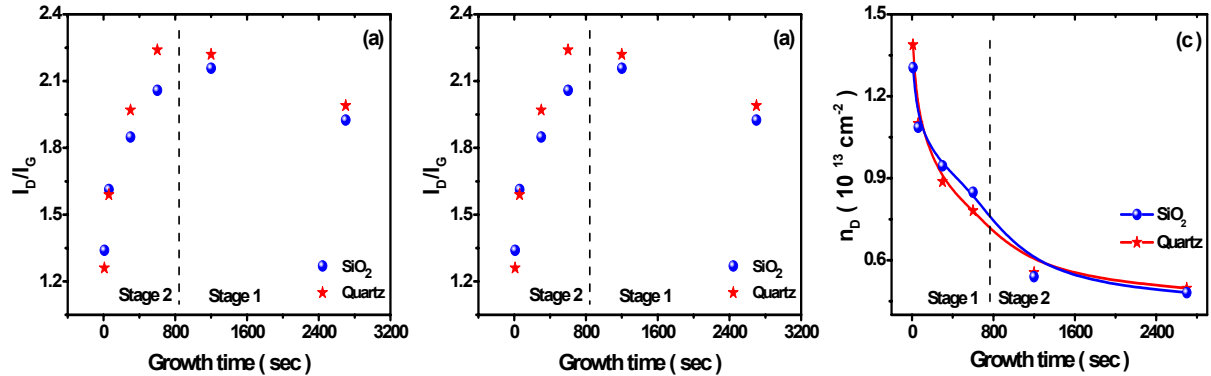


Fig.6- (a) The variation of I_D/I_G with respect to growth time (b) the plot of L_D versus I_D/I_G (c) the calculated defect density with growth time for the VGNs grown on quartz and SiO₂/Si substrates. The solid line in the Fig. 6b is the fit to the experimental data along with simulated curve with the same fitting parameters ($0 < L_D < 50$ nm). The fitting is performed using equation 5. The solid line in the Fig. 6c is guide to eye.

Cancado *et al* [25] developed a model to estimate the inter defect distance (L_D) and defect density (n_D) in ion bombarded graphene by Raman spectroscopy with appropriate boundary

conditions. According to the model, the L_D and n_D can be quantified in stage 1 and stage 2 as given below.

$$L_D^2(LD) = \frac{4.3 \times 10^3}{E_L^4} \left(\frac{I_D}{I_G} \right)^{-1} \quad \dots\dots\dots 1$$

$$L_D^2(HD) = 5.4 \times 10^{-2} E_L^4 \left(\frac{I_D}{I_G} \right) \quad \dots\dots\dots 2$$

$$n_D(LD) = (7.3 \times 10^9) E_L^4 \left(\frac{I_D}{I_G} \right) \quad \dots\dots\dots 3$$

$$n_D(HD) = \frac{5.9 \times 10^{14}}{E_L^4} \left(\frac{I_D}{I_G} \right)^{-1} \quad \dots\dots\dots 4$$

where E_L is the excitation energy of the laser. The equations 1 and 3 are valid for low (stage 1) defect concentration and the equations 2 and 4 are valid for high (stage 2) defect concentration regimes in the graphitic structure. By considering similar assumption [25], we calculated L_D (n_D) using equations 1(3) and 2(4) for films grown for > 10 mins and ≤ 10 mins respectively. Fig. 6b shows the variation of I_D/I_G with respect to L_D , exhibiting a non-monotonic behavior. The mechanism for such behavior is discussed earlier (Fig 6a). The non-monotonic trend was also observed for ion bombarded graphene and explained with a phenomenological model for quantifying ion-induced defects in graphene [26]. According to the model,

$$\frac{I_D}{I_G} = C_A \frac{r_A^2 - r_S^2}{r_A^2 - 2r_S^2} \left[\exp\left(\frac{-\pi r_S^2}{L_D^2}\right) - \exp\left(-\pi \frac{r_A^2 - r_S^2}{L_D^2}\right) + C_S \left(1 - \exp\left(\frac{-\pi r_S^2}{L_D^2}\right)\right) \right] \quad \dots\dots\dots 5$$

where C_A and C_S are the maximum possible value of I_D/I_G when the hexagonal network of carbon atoms are not disturbed and highly disordered limit respectively. The parameters r_A and r_S are the radius of defect activated region and structurally disordered region respectively (with $r_A > r_S$). The solid line in the Fig. 6b is the fit to the experimental data along with simulated curve with the same fitting parameters ($0 < L_D < 50$ nm) and finds an excellent agreement with the model. The best fit parameters are found to be $r_A=3.81$ nm, $r_S=1.08$ nm, $C_A=5.0$ and $C_S=0.4$ which are closely matching to the reported values [26]. The fitted curve indicates an initial increase of I_D/I_G

ratio up to a critical L_D value of about 3.8 nm and further monotonic decrease with increase in L_D [25-27]. Hence, this plot clearly indicates the transformation of defects and disorder with growth time which demonstrate the cross over from stage 2 to stage 1 of Ferrari and Robertson [30] model. Fig. 6c shows the variation of defect concentration with respect to growth time. As it can be seen from the figure 6c, the defect concentration continuously decreases with growth time. Thus, Raman studies verify the evolution of graphene nanosheets and reveal the type of defects present in two different substrates. It is found that the defect density is so high at early stage of growth due to the nano-graphite island formation. Later, the defect density monotonically decreases due to the formation of high pure VGNs. These observations are in excellent agreement with the growth mechanism as discussed in SEM analysis section 3.1.

3.3 XPS analysis

In order to strengthen the growth mechanism obtained from SEM and defect transformation at different stages obtained from Raman spectroscopy, XPS studies are carried out for the VGNs films grown on SiO_2/Si substrates. Fig. 7a shows the high resolution C1s XPS spectra of the films grown for 10 sec, 10 and 45 mins. The XPS spectra show a clear asymmetry in the higher binding energy (B.E.) regime for all the three samples, which is typically observed for high conductive metals and also the asymmetry increases with growth time. These observations confirm that the VGNs are highly conducting and of graphitic nature [31,32]. As seen in the Fig. 7a, the peak position of the C1s spectra are found to shift towards lower B.E. with growth time. The deconvoluted high resolution C1s spectrum of the film grown on SiO_2/Si for 10 mins is shown in Fig. 7b. The main peak ~ 284.4 eV corresponds to $\text{C}=\text{C}$ sp^2 bonded graphitic structure, and the one around 285.1 eV corresponds to defect structure arising from C-H related sp^3 bonded structure [14, 17, 33]. In addition, the peaks related to C-O, C=O bonding, probably from adsorbed impurities, are observed. This C-H related sp^3 bonded structure is also confirmed by FTIR spectroscopy which shows absorption peaks at around 2958 and 2875 cm^{-1} corresponding to the asymmetric and symmetric $\text{sp}^3\text{-CH}_3$ vibration respectively (results are not shown here) [34]. Note, there is also one more peak near 284.1 eV which is closely matching to the B.E. for Si-C alloy. In order to verify Si-C alloy formation at SiO_2 -nanographite interface during the nucleation process, Si2p XPS spectra are taken for all the three samples and are

shown in inset of Fig. 7c. As can be seen from Fig 7c, there is no evidence for the formation of Si-C, which should show a signature at around 100.8 eV. It should be noted that Raman measurements also did not show any evidence for Si-C formation, which should have a phonon mode at about 800 cm^{-1} . Hence, we exclude the phenomenon of Si-C formation which is reported in the literature [17, 35].

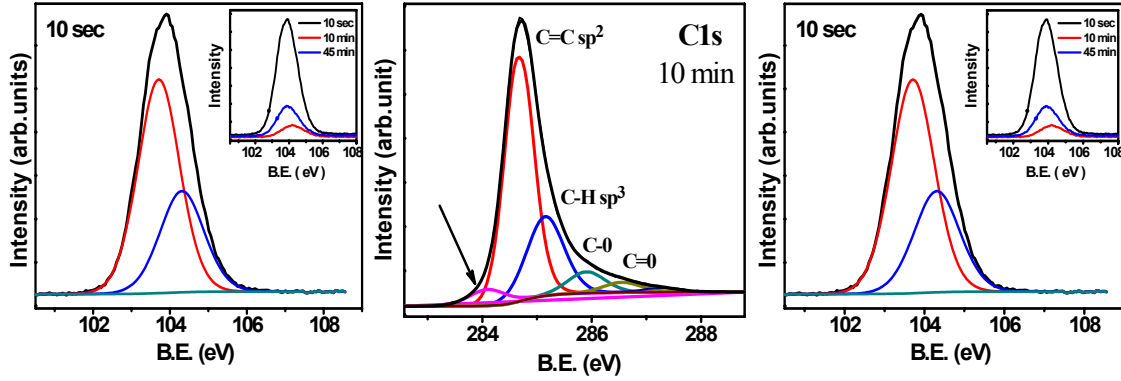


Fig.7- (a) the high resolution C1s spectra for the films grown for 10 sec, 10 min and 45 min (b) deconvulated C1s spectrum for the film grown for 10 min and (c) the Si2p XPS spectrum for 10 sec grown film. The inset in Fig. 7a is an extended region of C1s at higher B.E. The inset in Fig. 7c is the combined Si2p spectra for the three films studied here.

To account for the peak with chemical shift lower to B.E. of C1s, in the case of multiwalled carbon nanotubes, Barinov et al [36] had demonstrated that the peak is due to the vacancies and also they verified it on the intentionally introduced vacancy-like defects in highly oriented pyrolytic graphite. Hence, we assign the peak at around 284.1 eV to the presence of vacancy-like defects. The Raman analysis also indicates the existence of combined vacancy-like defects and hopping defects which is in an excellent agreement with XPS analysis. Moreover, the hopping defects and vacancies are closely related in disordered system because the hopping of charge carriers / atoms can take place on the vacancy sites [36]. As shown in Table 1, the B.E. of all peak positions ($\text{C}=\text{C sp}^2$, C-H sp^3 related defects, C-O , C=O , and vacancy-like defects) in the spectrum decreases with increase in growth time. Also, the area under the curves for defect related peaks continuously decreases which indicates the lowering of defect density with growth time. Further, as seen in inset of Fig. 7a, $\pi-\pi^*$ energy loss peak increases with growth time indicating the high conductive graphitic structure of the samples with time. These results confirm

the evolution of better graphitic structure with time. Further, electrical and optical studies are carried out and discussed below to support the study.

Table1. The parameters extracted from XPS analysis for the VGNs grown on SiO₂/Si substrate

Growth time	C=C sp ²		C-H sp ³ defect		C-O		C=O		Vacancy-like defects	
	BE (eV)	Area (%)	BE (eV)	Area (%)	BE (eV)	Area (%)	BE (eV)	Area (%)	BE (eV)	Area (%)
10 sec	284.71	45.24	285.21	36.19	286.00	6.67	286.65	3.81	284.2	6.67
10 min	284.65	59.81	285.15	24.30	285.90	6.54	286.55	3.11	284.1	4.98
45 min	284.55	60.12	285.04	25.30	285.75	6.54	286.45	3.12	283.9	3.57

3.4 Electrical and optical properties of VGNs

Fig. 8a shows the room temperature sheet resistance of the VGNs grown on SiO₂/Si with respect to growth time. The sheet resistance decreases from 30 to 2.17 kΩ/□ with increasing growth time and it shows an ohmic behaviour in I-V characteristics under low bias condition (as shown in inset of Fig 8a). The decreasing resistance is mainly due to the growth of the high pure and high conductive few layer VGNs networks over the relatively high resistive nanographite film. As the growth time increases, the length and height of the VGNs increases with decrease in defect density as evidenced from Raman and XPS analysis. Hence, the sheet resistance decreases with growth time due to the domination of conducting pure VGNs. The optical transmittance in UV-Vis range from 200 to 800 nm is recorded for the samples grown on quartz substrates and shown in Fig. 8b. The inset in Fig 8b shows the optical transmittance at 550nm over growth time and it varies from 95 to 78 %. The samples grown for 10 sec exhibits very high optical transmittance and it decreases with time due to the increase in thickness as well as the high conducting nature of the VGNs. All the films show a strong absorption at about 270 nm which is due to the π - π^* transition in graphitic system and the increased absorption with time indicate improved graphitic nature of the films.

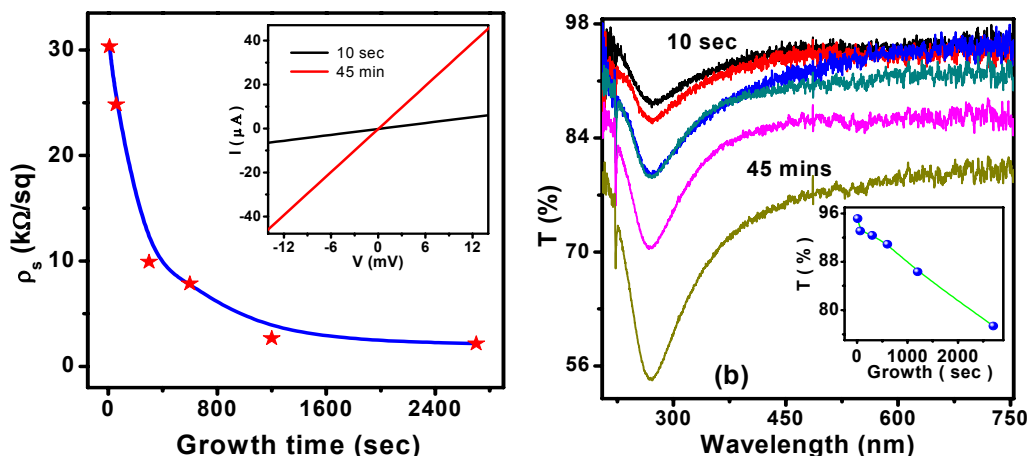


Fig.8. (a) The variation of sheet resistance of VGNs grown on SiO₂/Si substrate and (b) UV-Vis transmission spectra of VGNs grown on quartz substrate with respect to growth time. The inset in Fig. 8(b) shows optical transmittance at 550 nm. The solid line in Fig. 8a is guide to eye.

4. Conclusion

A catalyst-free direct synthesis of VGNs has been demonstrated by ECR-CVD at a relatively low substrate temperature on SiO₂/Si and quartz substrates. Our experimental observations suggest that the growth mechanism is based on the direct adsorption and surface diffusion of carbon species rather than the carbide formation at the interface. For the first time, we have identified the type of defects and the transformation of defects for the VGNs grown by plasma based systems. The transformation of defects with growth time is in conceptual agreement with a well established amorphization trajectory for graphitic materials. The VGNs grown on SiO₂/Si substrates contains predominantly combined vacancy-like and hopping defects. On the other hand, the VGNs grown on quartz substrates contain mainly boundary-like defects. Further, the amount of defects considerably decreases with growth time grown on both the substrates. The XPS studies carried out on SiO₂/Si substrates also support the existence of vacancy-like defects. Moreover, the area under the curve for XPS defect peaks monotonically decrease with growth time indicates that the defect density decreases with growth time. Further, the grown films show an excellent transmittance and low sheet resistance. The improved understanding over the growth mechanism, defect analysis and their correlation with electrical

and optical properties would help to develop the films with desired characteristics which are needed for microelectronics and optoelectronic applications.

References

- [1] Dresselhaus M S 1997 Future directions in carbon science. *Annu. Rev. Mat. Sci.* **27**(1) 1-34
- [2] Bellucci S and Malesevic A 2011 Physics of Carbon Nanostructures. In: Bellucci S, editor, Physical Properties of Ceramic and Carbon Nanoscale Structures. *Springer-Verlag Berlin Heidelberg* **11** 155-94
- [3] Geim A K and Novoselov K S 2007 The rise in graphene *Nat. Mater.* **6** 183-191
- [4] Sharma S D, Adam S, Hwang E H and Rossi E 2011 Electronic transport in two-dimensional graphene. *Rev. Mod. Phys.* **83** 407-70
- [5] Wu Y H, Yu T and Shen Z X 2010 Two-dimensional carbon nanostructures: Fundamental properties, synthesis, characterization, and potential applications. *J. Appl. Phys.* **108** 071301
- [6] Singh V, Joung D, Zhai L, Das S, Khondaker S I and Seal S 2011 Graphene based materials: Past, present and future *Prog. Mat. Sci.* **56** 1178–1271
- [7] Mattevi C, Kim H and Chhowalla M 2011 A Review of chemical vapor deposition of graphene on copper *J. Mater. Chem.* **21** 3324-3334
- [8] Pirkle A, Chan J, Venugopal A, Hinojos D, Magnuso C W, McDonnell S, Colombo L, Vogel E M, Ruoff R S and Wallace R M 2011 The effect of chemical residues on the physical properties and electrical properties of chemical vapor deposited graphene transferred to SiO₂ *Appl. Phys. Lett.* **99** 122108
- [9] Wang D, He T, Yang Y, Xie D, Ren T L and Zhang Y 2013 Scalable and Direct Growth of Graphene Micro Ribbons on Dielectric Substrates *Scientific Reports* **3** 1348
- [10] Yan Z, Peng Z, Sun Z, Yao J, Zhu Y, Liu Z, Ajayan P M and Tour J M 2011 Growth of Bilayer Graphene on Insulating Substrates *ACS Nano* **5**(10) 8187-8192
- [11] Bo Z, Yang Y, Chen J, Yu K, Ya J and Cen K 2012 Plasma-enhanced chemical vapor deposition synthesis of vertically oriented graphene nanosheets *Nanoscale* **5** 5180-204
- [12] Hiramatsu M, Kondo H and Hori M 2013 Graphene Nanowalls, Nanotechnology and nanomaterials “New progress on Graphene Research”, editor Jian Ru Gang, 235-60. DOI: 10.5772/51528. ISBN 978-953-51-1091-0

- [13] Quinlan R A, Cai M, Outlaw R A, Butler S M, Miller J R and Mansour A N 2013 Investigation of defects generated in vertically oriented graphene *Carbon* **64** 92-100
- [14] Shang N G, Papakonstantinou P, McMullan M, Chu M, Stamboulis A, Potenza A, Dhesi S S and Marchetto H 2008 Catalyst-Free Efficient Growth, Orientation and Biosensing Properties of Multilayer Graphene Nanoflake Films with Sharp Edge Planes *Adv. Funct. Mater.* **18** 3506-14
- [15] Wu Y, Qiao P, Chong T and Shen Z 2002 Carbon Nanowalls Grown by Microwave Plasma Enhanced Chemical Vapor Deposition *Adv. Mat.* **14** 64 -67
- [16] Zhang L, Shi Z, Wang Y, Yang R, Shi D and Zhang G 2011 Catalyst-Free Growth of Nanographene Films on Various Substrates *Nano. Res.* **4**(3) 315-21
- [17] Medina H, Lin Y C, Jin C, Lu C C, Yeh C H, Huang K P, Suenaga K, Robertson J and Chiu P W 2012 Metal-Free Growth of Nanographene on Silicon Oxides for transparent electrode application *Adv. Funct. Mater.* **22** 2123-2128
- [18] Kim J, Heo S B, Gu G H and Suh J S 2010 Fabrication of graphene flakes composed of multi-layer graphene sheets using a thermal plasma jet system *nanotechnology* **21** 095601
- [19] Yoshimura A, Yoshimura H, Shin S C, Kobayashi K, Tanimura M and Tachibana M 2012 Atomic force microscopy and Raman spectroscopy study of the early stages of carbon nanowall growth by dc plasma-enhanced chemical vapor deposition *Carbon* **50** 2698-702
- [20] Kondo S, Kawai S, Takeuchi W, Yamakawa K, Den S, Kano H, Hiramatsu M and Hori M 2009 Initial growth process of carbon nanowalls synthesized by radical injection plasma-enhanced chemical vapor deposition *J. Appl. Phys.* **106** 094302
- [21] Ferrari A C and Basko D M 2013 Raman spectroscopy as a versatile tool for studying the properties of graphene *Nat. Nanotech.* **8** 235-46
- [22] Gilkes K W R, Sands H S, Batchelder D N, Robertson J and Milne W I 1997 Direct observation of sp³ bonding in tetrahedral amorphous carbon using ultraviolet Raman spectroscopy *Appl. Phys. Lett.* **70** 1980
- [23] Casiraghi C 2009 Probing disorder and charged impurities in graphene by Raman spectroscopy *Phys Status Solidi RRL* **3**(6) 175-7
- [24] Ferreira E H M, Moutinho M V O, Stavale F, Lucchese M M, Capaz R B, Achete C A and Jorio A. 2010 Evolution of the Raman spectra from single-, few-, and many-layer graphene with increasing disorder *Phy. Rev. B* **82** 125429.

- [25] Cancado L G, Jorio A, Ferreira E H M, Stavale F, Achete C A, Capaz R, Moutinho M V O, Lombardo A, Kulmala T S and A. C. Ferrari 2011 Quantifying Defects in Graphene via Raman Spectroscopy at Different Excitation energies *Nano Letter.* **11** 3190-96
- [26] Lucchese M M, Stavale F, Ferreira E H M, Vilani C, Moutinho M V O, Capaz R B, Achete C A and Jorio A 2010 Quantifying ion-induced defects and Raman relaxation length in graphene *Carbon* **48** 1592-97
- [27] Jorio A, Ferreira E H M, Moutinho M V O, Stavale F, Achete C A and Capaz R B 2010 Measuring disorder in graphene with the G and D bands *Phys Status Solidi B* **247** 2980-2
- [28] Venezuela, P Lazzeri M and Mauri F 2011 Theory of double-resonant Raman spectra in graphene: Intensity and line shape of defect-induced and two-phonon bands *Phys. Rev. B* **84** 035433
- [29] Eckmann A, Felten A, Mishchenko A, Britnell L, Krupke R, Novoselov K S and Casiraghi C 2012 Probing the nature of defects in Graphene by Raman Spectroscopy *Nano Lett.* **12**(8) 3925-30
- [30] Ferrari A C and Robertson J 2000 Interpretation of Raman spectra of disordered and amorphous carbon *Phys. Rev. B* **61** 14095-14107
- [31] Peltekis N, Kumar S, McEvoy N, Lee K, Weidlich A and Duesberg G S 2012 The effect of downstream plasma treatments on graphene surfaces *Carbon* **50** 395-403
- [32] Cheung T T P 1982 X-ray photoemission of carbon: Lineshape analysis and application to studies of coals *J. Appl. Phys.* **53** 6857-62
- [33] Nikitin A, Näslund L A, Zhang Z and Nilsson A 2008 C–H bond formation at the graphite surface studied with core level spectroscopy *Surf. Sci.* **602** 2575–80.
- [34] Dischler B, Bubenzer A and Koidl P 1983 Bonding in hydrogenated hard carbon studied by optical spectroscopy *Solid State Comm.* **48** 105-08
- [35] Malesevic A, Vitchev R, Schouteden K, Volodin A, Zhang L, Tendeloo G V, Vanhulsel A and Haesendonck C V 2008 Synthesis of few-layer graphene via microwave plasma-enhanced chemical vapour deposition *Nanotechnology* **19** 305604
- [36] Barinov A, Üstünel H, Fabris S, Gregoratti L, Aballe L, Dudin P, Baroni S and Kiskinova M 2007 Defect-Controlled Transport Properties of Metallic Atoms along Carbon Nanotube Surfaces *Phys. Rev. Lett.* **99** 046803